Latent Fingerprint Enhancement via Robust Orientation Field Estimation

Soweon Yoon[†], Jianjiang Feng[‡], and Anil K. Jain[†*]
[†]Dept. of Computer Science and Engineering
Michigan State University, U.S.A.
{yoonsowo,jain}@cse.msu.edu
[‡]Dept. of Automation
Tsinghua University, Beijing, China
jfeng@tsinghua.edu.cn

Abstract

Latent fingerprints, or simply latents, have been considered as cardinal evidence for identifying and convicting criminals. The amount of information available for identification from latents is often limited due to their poor quality, unclear ridge structure and occlusion with complex background or even other latent prints. We propose a latent fingerprint enhancement algorithm, which expects manually marked region of interest (ROI) and singular points. The core of the proposed algorithm is a robust orientation field estimation algorithm for latents. Short-time Fourier transform is used to obtain multiple orientation elements in each image block. This is followed by a hypothesize-and-test paradigm based on randomized RANSAC, which generates a set of hypothesized orientation fields. Experimental results on NIST SD27 latent fingerprint database show that the matching performance of a commercial matcher is significantly improved by utilizing the enhanced latent fingerprints produced by the proposed algorithm.

1. Introduction

Automated Fingerprint Identification Systems (AFIS) have been successfully used in forensics and law enforcement applications to reliably identify an individual. Fingerprint matching scenarios generally fall into one of the following two categories: (i) tenprint search and (ii) latent search. In tenprint search, rolled and plain impressions of a subject's fingers are searched against the tenprint fingerprint database. Rolled fingerprint images are obtained by rolling a finger from one side to the other ("nail-to-nail") in order to capture all the ridge details of a finger (Fig. 1a). Plain fingerprints are acquired by pressing a fingertip onto a flat surface of either a paper for inking methods or a flatbed of a live-scan device (Fig. 1b). While rolled fingerprints contain a large number of minutiae (about 100), plain fingerprints capture relatively small finger area with smaller number of minutiae (about 50) and lower skin distortion than rolled prints. The matching performance of the AFIS for tenprint search has reached a satisfactory level in most fingerprint recognition applications. In 2003 Fingerprint Vendor Technology Evaluation (FpVTE) [10], the best rank-1 identification rate of the commercial matchers was already 99.4% on a database of 10,000 plain fingerprints.

Latent fingerprints (see Fig. 1c), which are lifted from the surface of objects touched or handled by a person, are an extremely important source of evidence in crime scene investigation to identify and convict the suspects. However, latent search is still a challenging problem due to their poor quality. The latent fingerprints contain partial area of a finger, and often have smudged or blurred ridges [3] and large nonlinear skin distortion due to pressure variations. In current practice of latent matching, the examiners manually mark minutiae and region of interest (ROI), search the input latent against a large database using AFIS, and then investigate top K (typically, $K = 50$) candidates retrieved from the database by manually comparing minutiae as well as Level 3 features such as pores, dots, incipient ridges, etc., if they are visible.

The success of the AFIS in forensics and law enforcement agencies worldwide is based on the availability of a large database of rolled and plain prints of the ten fingers of all apprehended criminals. As a result, the size of

(a) (b) (c)

Figure 1. Three types of impressions of the same finger. (a) Rolled fingerprint, (b) plain fingerprint, and (c) latent fingerprint.

*A. K. Jain is also with the Dept. of Brain and Cognitive Engineering, Korea University, Anam-dong, Seongbuk-gu, Seoul 136-713, Korea.

the background database is huge and is constantly increasing; currently, FBI's IAFIS fingerprint database contains the records of about 70 million subjects. Therefore, for latent search, a "Lights-Out" identification mode is desirable. "Lights-Out" latent fingerprint identification refers to a system which accepts a latent image as input and returns a short list of candidates from the database with no human intervention [1]. In a recent NIST report on the Evaluation of Latent Fingerprint Technologies (ELFT) [7], the most accurate latent matcher achieved 66.7% rank-1 identification rate in matching 1,114 latents against 100,000 rolled and plain tenprint cards when the latent image and the full feature set marked by latent examiners were available as input to the matcher.

The primary focus in developing automatic latent identification algorithms is to reduce the human intervention to as little as possible while preserving the matching accuracy with full manual markup. Automatic fingerprint feature extractors designed for rolled/plain prints do not work properly on latents since many true minutiae are likely to be missed due to low ridge clarity and many spurious minutiae are likely to be extracted due to background noise. In this paper, we propose an automatic latent fingerprint enhancement algorithm which requires minimal markup - ROI and singular points (i.e., core and delta). Note that we do not require a latent examiner to mark minutiae or ridges which demand significant effort. The objectives of the latent fingerprint image enhancement are to: (i) improve automatic feature extraction and matching performance of latent fingerprints, and (ii) provide visually enhanced images for latent examiners to mark fingerprint features better.

2. Latent Enhancement

Estimating orientation field of a fingerprint is a crucial stage in most fingerprint matching algorithms. Orientation field, $\theta(x, y)$, represents the ridge flow of a fingerprint at each location. To reduce computational and storage complexity, fingerprint orientation field is generally defined at the block level rather than at the pixel level. The dominant ridge orientations in a block are called *orientation elements* and defined in the interval $[0, \pi)$. Quality of fingerprint ridges can be improved by enhancing the local ridge clarity along the ridge orientation and suppressing noise in other directions. The proposed latent fingerprint enhancement algorithm consists of the following four steps:

1. Manual markup of ROI and singular points.
2. Orientation element computation using the short-time Fourier transform (STFT).
3. Orientation field estimation using R-RANSAC.
4. Fingerprint enhancement using Gabor filters [6].

Details of steps 1-3 are described in the following sections.

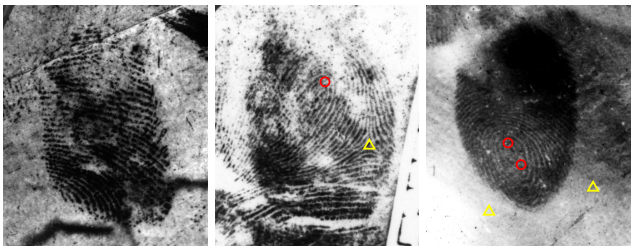

(a) (b) (c)

Figure 2. Manual markup of singular points. (a) No singularities are present, (b) two real singular points, and (c) two real cores and two virtual deltas.

2.1. Manual Markup

We assume that the following information is manually marked by fingerprint examiners: (i) fingerprint region in the latent image, or the region of interest (ROI), and (ii) singular points. ROI is a closed region that is bounded at the outermost trim of the latent. Only the fingerprint features in the ROI are regarded as valid.

Singularities observed in almost all the fingerprints fall into one of the following categories: (i) no singularity (i.e., arch type of fingerprints), (ii) one core and one delta (i.e., loop and tented arch type), and (iii) two cores and two deltas (i.e., whorl and twin loop type). Note that not all singular points may be observed in a given fingerprint image; for example, plain impression tends to capture only the central area of a finger. Based on this observation, latent examiners are expected to mark singular points using the following convention:

- If the latent does not contain any singularity, no singular points are marked (see Fig. 2a). Even though a latent fingerprint may in fact come from a finger with singularity, the latent will be treated as plain arch, the simplest fingerprint pattern.
- If the latent contains singular points, cores and deltas should be marked in pairs. For example, the latent fingerprint in Fig. 2b has one core and one delta in ROI. These singular points are called *real* singular points since they are present in the ROI. On the other hand, when the numbers of core and delta are not equal, the missing singular points are marked with the best guess. These are called *virtual* singular points since they are not observable in the ROI. For example, the latent in Fig. 2c contains only two real cores and the two virtual deltas are also marked with the best guess.

2.2. Orientation Element Computation

Fingerprint ridges in a local image block generally contain only one dominant orientation. A popular approach to

(a) (b)

Figure 3. Orientation elements extracted from a latent using STFT. (a) Latent (NIST SD27, G027) and (b) orientation elements.

compute the orientations in a block is based on the short-time Fourier transform (STFT) [4], which detects the peaks in the magnitude spectrum of the local image. However, in latent fingerprints, multiple local maxima may appear in the magnitude spectrum due to the structured background noise such as lines (see Fig. 3a), and the peak corresponding to the fingerprint ridges can be easily confused with the peaks corresponding to the structured noise. Thus, we compute multiple dominant orientations (orientation elements) in each block and determine the true ridge orientation in the next stage. Fig. 3b shows the extracted orientation elements in each block in the ROI from the latent in Fig. 3a.

For each local block of 16×16 pixels in the ROI, the orientation elements are computed as follows:

1. Compute the Fourier transform of a local image block (see Figs. 4a and b).
2. Multiply the magnitude spectrum of the image with a set of directional filters (Fig. 4c) in Fourier domain; each directional filter is constructed by multiplying a binary mask (1 for $\theta \in \left[\frac{\pi}{L}\left(i-\frac{1}{2}\right), \frac{\pi}{L}\left(i+\frac{1}{2}\right)\right)$, $i = 0, 1, \ldots, L-1$) and a band-pass filter whose frequency range includes possible fingerprint ridge frequencies. $L = 8$ is selected.
3. Sum the energy for each filtered response (Fig. 4d).
4. Find peaks (local maxima) in the one-dimensional energy plot. Orientation corresponding to the peak from the i-th directional filter is $\left[\frac{\pi}{L}i + \frac{\pi}{2}\right] \bmod \pi$.

Fig. 4e shows two orientation elements extracted from the image block in Fig. 4a.

2.3. Orientation Field Estimation

In this stage, we use a two-level approach to estimate the orientation field of a latent: (i) the orientation elements in a neighborhood are merged into an orientation group whose elements are compatible each other, and (ii) a global orientation field is robustly estimated by a set of orientation groups. The following sections describe the orientation field model and the details in orientation field estimation algorithm.

2.3.1 Orientation Field Model

Orientation field, $\theta(x, y)$, of fingerprint can be decomposed into two components:

$$\theta(x, y) = [\theta_s(x, y) + \theta_r(x, y)] \mod \pi, \tag{1}$$

where $\theta_s(x, y)$ represents the singular orientation field and $\theta_r(x, y)$ represents the residual orientation field.

Singular orientation field, $\theta_s(x, y)$, describes the abstract ridge flow determined by only the singular points (i.e., cores and deltas) [9] where fingerprint orientation field changes abruptly. The singular orientation field is obtained by:

$$\theta_s(z) = \left[\frac{1}{2}\arg\left(e^{i2\theta_\infty}\frac{(z-z_{c_1})(z-z_{c_2})\cdots(z-z_{c_m})}{(z-z_{d_1})(z-z_{d_2})\cdots(z-z_{d_m})}\right)\right] \bmod \pi. \tag{2}$$

where $z = x + iy$, $\{z_{c_j}\}$ and $\{z_{d_j}\}$ are the positions of cores and deltas, and θ_∞ is the orientation at infinity.

Residual orientation field, $\theta_r(x, y)$, represents natural changes in ridge flow of a fingerprint that are not influenced by the singularities; it is continuous everywhere. A set of polynomials can represent the sine and cosine part of the residual orientation field as follows:

$$g_c^n(x, y) \triangleq \cos 2\theta_r(x, y) = \sum_{i=0}^{n}\sum_{j=0}^{i} a_{i,j}x^j y^{i-j}, \tag{3}$$

$$g_s^n(x, y) \triangleq \sin 2\theta_r(x, y) = \sum_{i=0}^{n}\sum_{j=0}^{i} b_{i,j}x^j y^{i-j}, \tag{4}$$

where $\{a_{i,j}\}$ and $\{b_{i,j}\}$ are the polynomial coefficients for $g_c^n(x, y)$ and $g_s^n(x, y)$, respectively. The order of the polynomials is set as 4 (i.e., $n = 4$).

Fig. 5 shows an example where the orientation field model is applied to a fingerprint. It indicates that the above model can successfully represent the orientation field of a fingerprint.

2.3.2 Orientation Element Grouping

Neighboring orientation elements which are compatible with each other are grouped in order to facilitate the subsequent orientation field estimation. Based on the continuity of the residual orientation field, compatible orientation elements are grouped together and a unique label is assigned to each group. Let $\theta_r^{(i)}(x, y)$, for $i = [1, \ldots, L(x, y)]$, be the i-th residual orientation element at (x, y), and $\mathcal{L}^{(i)}(x, y)$ be the label assigned to this orientation element. Initially, $\mathcal{L}^{(i)}(x, y) = 0$ for all i and (x, y). Orientation element grouping starts from the elements which are the only dominant orientation in a block; they become seed points. For

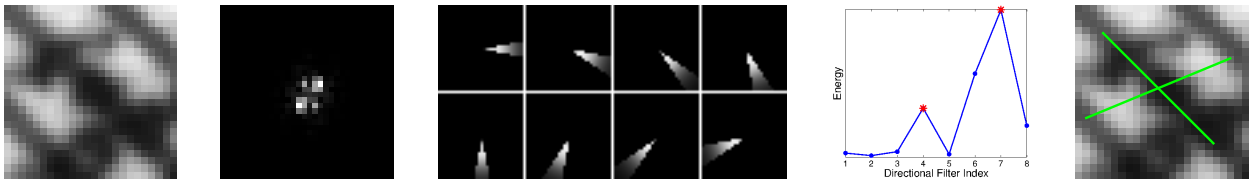

(a) (b) (c) (d) (e)

Figure 4. Orientation element computation. (a) A local image block, (b) magnitude spectrum of (a), (c) directional filters, (d) energy of filtered responses by each directional filter, and (e) two orientation elements in this local block that correspond to the two peaks in (d).

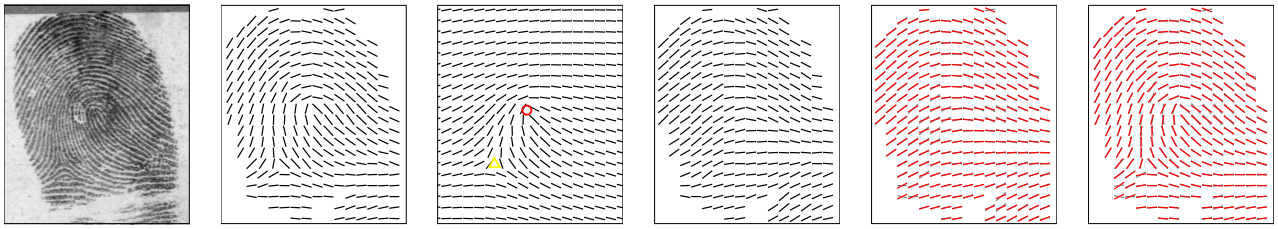

(a) (b) $\theta(x,y)$ (c) $\theta_s(x,y)$ (d) $\theta_r(x,y)$ (e) $\hat{\theta}_r(x,y)$ (f) $\hat{\theta}(x,y)$

Figure 5. Orientation field model. (a) Fingerprint (NIST SD4, F0004), (b) orientation field extracted from (a), (c) singular component of the orientation field, (d) residual component of the orientation field, (e) modeled residual orientation field using the 4th order polynomial model, and (f) reconstructed orientation field, $\hat{\theta}(x,y) = \theta_s(x,y) + \hat{\theta}_r(x,y)$.

a seed point $\theta_r^{(i)}(x,y)$, a neighboring orientation element $\theta_r^{(j)}(x',y')$ is deemed as a candidate to belong to the same group as this seed point if (i) $\mathcal{L}^{(j)}(x',y') = 0$: no label is yet assigned to this neighboring orientation element; (ii) the distance between two blocks is within 5 blocks; and (iii) $|\theta_r^{(i)}(x,y) - \theta_r^{(j)}(x',y')| < \pi/2L$: the orientation difference is less than the threshold.

The candidates which are 4-connected to the seed point (i.e., a 4-connected path can be found among the set of candidates) are assigned the same label as the seed point. Once all the seed points are grouped, the orientation elements which are the only one unlabeled element in a block become new seed points. This procedure is repeated until every orientation element has been assigned a label. Fig. 6 shows five of the orientation element groups in a latent fingerprint.

2.3.3 Hypotheses Generation

Given a set of orientation element groups as the input, hypotheses for residual orientation field are built based on the randomized Random Sample Consensus (R-RANSAC) algorithm [8]. Generally, RANSAC algorithms consist of three basic steps: (i) select a set of initial data points randomly, (ii) build a hypothesis, and (iii) evaluate the hypothesis. A set of data points that are consistent with a given hypothesis is called *consensus set*. The differences between R-RANSAC and the basic RANSAC are: (i) the number of initial data points selected is more than the minimum number of points required to build a hypothesis, and (ii) the hypothesis evaluation against all data points is conducted only if all initial data points are consistent with the hypothesis.

Let G be the set of all orientation elements and N be the total number of the orientation groups. An orientation group is randomly selected from G based on the following probability density function (pdf) which is constructed from the area of each group. The probability for random selection, p_i, of the i-th group with area A_i is defined as:

$$p_i = A_i / \sum_{j=1}^{N} A_j. \tag{5}$$

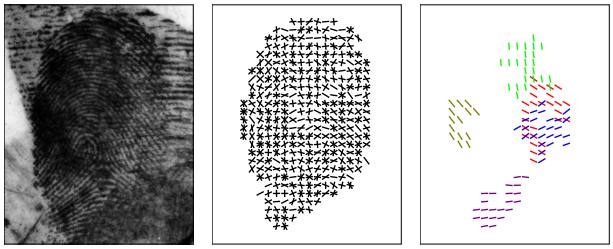

(a) (b) (c)

Figure 6. Orientation element grouping. (a) Fingerprint (NIST SD27, G017), (b) residual orientation elements, and (c) five orientation element groups, each shown in a different color.

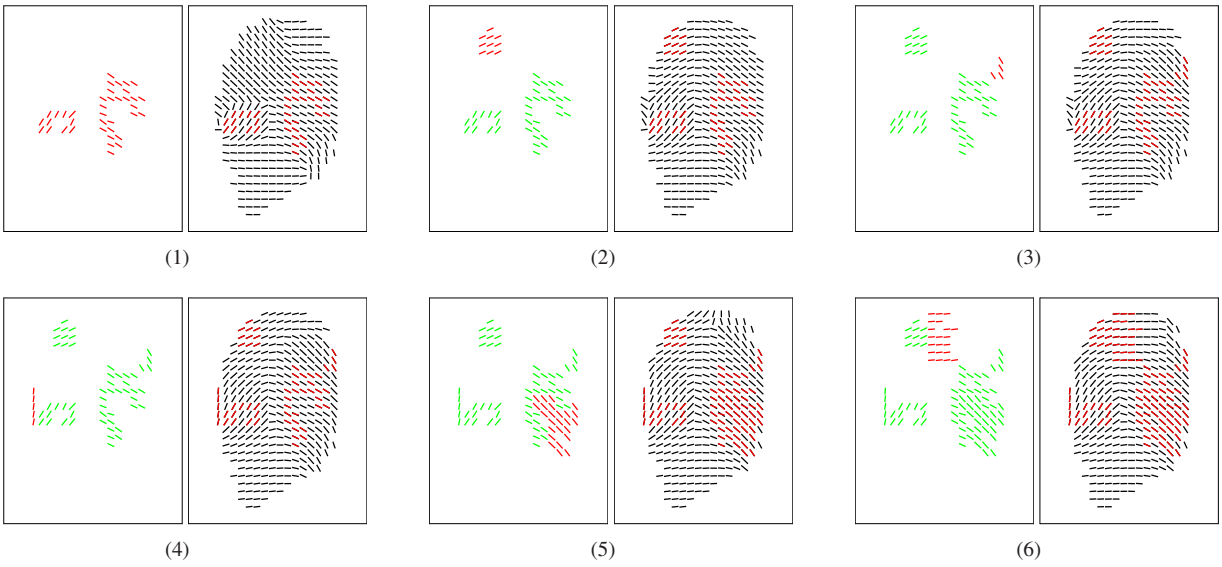

Figure 7. One iteration of hypothesis generation procedure for the latent in Fig. 6. An orientation group is newly added to S at each step from (1) to (6) (newly added groups are marked as red and existing groups in S are marked green in the left image of each pair); a hypothesis is built at every update in S and checked if S are all consistent with the hypothesis (red blocks in right images indicate consistent S). The final hypothesis M is obtained at the end of the iteration when there are no more groups can be added to S. Then, M in (6) is evaluated by checking the existence of singularity (see Fig. 8).

Orientation elements in the selected group are added to a set S; the size of S increases monotonically during an iteration. Initially, non-overlapping orientation groups are selected randomly according to the pdf until the size of S is greater than the minimum number of data points (m) to build a hypothesis; m is 15 for the 4th order polynomial.

Once the size of S is greater than m, a hypothesis is built using all orientation elements in the current S. The hypothesized model refers to the coefficients of the polynomials, $\{a_{i,j}\}$ and $\{b_{i,j}\}$, in Eqs. (3) and (4) which are obtained using least-squares estimation by minimizing

$$\sum\nolimits_{\theta_r^{(i)}(x,y)\in S} |g_c^n(x,y) - \cos 2\theta_r^{(i)}(x,y)|^2, \qquad (6)$$

$$\sum\nolimits_{\theta_r^{(i)}(x,y)\in S} |g_s^n(x,y) - \sin 2\theta_r^{(i)}(x,y)|^2. \qquad (7)$$

If all orientation elements in S are within some error tolerance of the hypothesis (π/L), the consensus set S^* is determined by testing the hypothesis against all orientation elements in G and this hypothesis is recorded if the size of the S^* is the largest in this iteration. The current iteration continues by adding a new non-overlapping orientation group to S. Fig. 7 shows the procedure of hypothesis generation for an iteration.

If not all orientation elements in S are consistent with the hypothesis, one of the following two actions is taken: (i) if the inconsistent group is the most recently added one, remove this group from S, add a new group to S, and continue the current iteration; (ii) otherwise, terminate the iteration and evaluate the best hypothesis at this iteration. Action (ii) is taken when no more non-overlapping orientation groups are found to be added in S.

The best hypothesis at each iteration is verified by checking if the hypothesized residual orientation field includes any singularity in the ROI. Singularities are found using Poincaré index [2]. The hypothesis is accepted if there is no singularity present in the ROI. Fig. 8 shows an accepted hypothesis, and the reconstructed orientation field combining the hypothesized residual orientation field with singular orientation field represents the true ridge flow well. If the hypothesized residual orientation field contains any singularity, it is rejected (see Fig. 9).

The algorithm terminates when the number of iterations exceeds (i) a predetermined maximum number of trials, or (ii) the minimum number of trials k satisfying [5]

$$k \geq \frac{\log(1-p_f)}{\log(1-\varepsilon^m)}, \qquad (8)$$

where p_f is the desired probability of having at least one S that consists of all orientation groups from the target latent fingerprint and ε is the true fraction of orientation elements from the latent in G. Since ε is typically unknown, it is updated with the size of the best consensus set during iterations.

Once the top-10 best candidate hypotheses for the orientation field are found, the latent fingerprint is enhanced

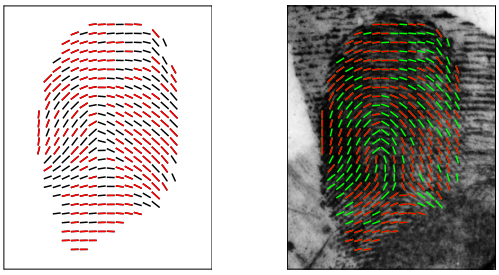

(a) (b)

Figure 8. Accepted hypothesis. (a) Accepted hypothesized residual orientation field and (b) reconstructed orientation field using (a). Red blocks in (a) and (b) indicate the consensus set.

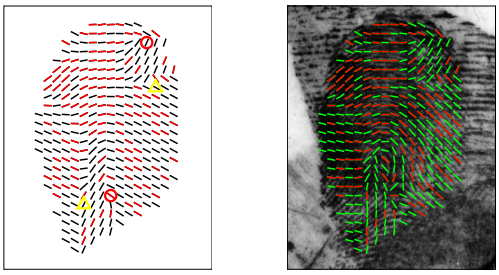

(a) (b)

Figure 9. Rejected hypothesis. (a) Rejected hypothesized residual orientation field with singularities (red circle for core and yellow triangle for delta) and (b) reconstructed orientation field using (a).

using Gabor filters [6] whose orientations are tuned to each orientation field hypothesis and whose frequencies are set to a fixed value (1/8 ridges per pixel). All ten enhanced latents are input to the fingerprint matcher. Then, the ten match scores output by the matcher are fused by the max rule.

Algorithm. Hypotheses Generation for Orientation Field Estimation

m: minimum number of blocks to build a hypothesis.
G: the set of orientation elements in all groups.
S: a set of orientation elements in selected groups (initially, S is empty).
p_i for $i = 1, \ldots, N$: a pdf for random selection.

I. Hypothesis

1. Initial S: Non-overlapping groups are selected randomly based on the given p such that the total number of orientation elements in S is greater than m.
2. Build a hypothesis M: $\{a_{i,j}\}$ and $\{b_{i,j}\}$ are estimated by the least-squares estimation using S.
3. If all orientation elements in S are consistent with the M, go to step 4. If the inconsistent orientation elements are only from the most recently added group, discard this group from S and go to step 5. Otherwise, go to step 6.
4. Find the consensus set S^*: S^* is determined by a subset of G which are within some error tolerance of the regularized residual orientation field from M. If $|S^*| > |S_{best}|$, update S_{best} and M_{best} with S and M. Go to step 5.
5. Add a group to S which is selected randomly in G and not overlapped with any orientations in S and go back to step 2. If there is no groups to be added, go to step 6.
6. Accept/reject the hypothesis: Check if the regularized residual orientation field from the hypothesis M_{best} contains any singularity [2]. If singularity exists in the ROI, reject the hypothesis. Otherwise, proceed to evaluation phase.

II. Evaluation

The accepted hypothesis is ranked in a descending order according to the size of the consensus set S^*_{best}.
Go back to I.

III. Output

Top-10 best hypotheses are retrieved from the accepted hypotheses.

3. Experimental Results

3.1. Database

The experiments are conducted on the public domain latent fingerprint database, NIST SD27, which contains 258 latent fingerprints and their corresponding rolled fingerprints. Each latent image in this database was assigned one of three (subjective) quality levels - *good*, *bad*, and *ugly* - by latent fingerprint examiners. The numbers of "good", "bad" and "ugly" latents are 88, 85 and 85, respectively. To make the latent matching problem more realistic and challenging, the background database was extended to 27,258 fingerprints by including 27,000 rolled prints in NIST SD14.

3.2. Performance Evaluation

The accuracy of the proposed latent fingerprint enhancement algorithm is evaluated by measuring latent matching performance using a commercial matcher, Neurotechnology VeriFinger SDK 4.2. The Cumulative Match Characteristic (CMC) curves of four types of the input to the fingerprint matcher are shown in Fig. 10. These inputs are: (i) enhanced latent by manually marked orientation field; (ii) enhanced latent by the estimated orientation field using the proposed algorithm; (iii) enhanced latent by the estimated orientation field using least-squares method [11]; and (iv) latent image with no enhancement.

Note that the performance of using manually marked orientation field provides the upper bound. As shown in Fig. 10a, the automatic matching performance is significantly improved when the enhanced images are used as input to the matcher. Furthermore, the proposed algorithm based on R-RANSAC performs better than least-squares estimation. The CMC curves are also shown separately according to the quality of the latents. For good quality latents,

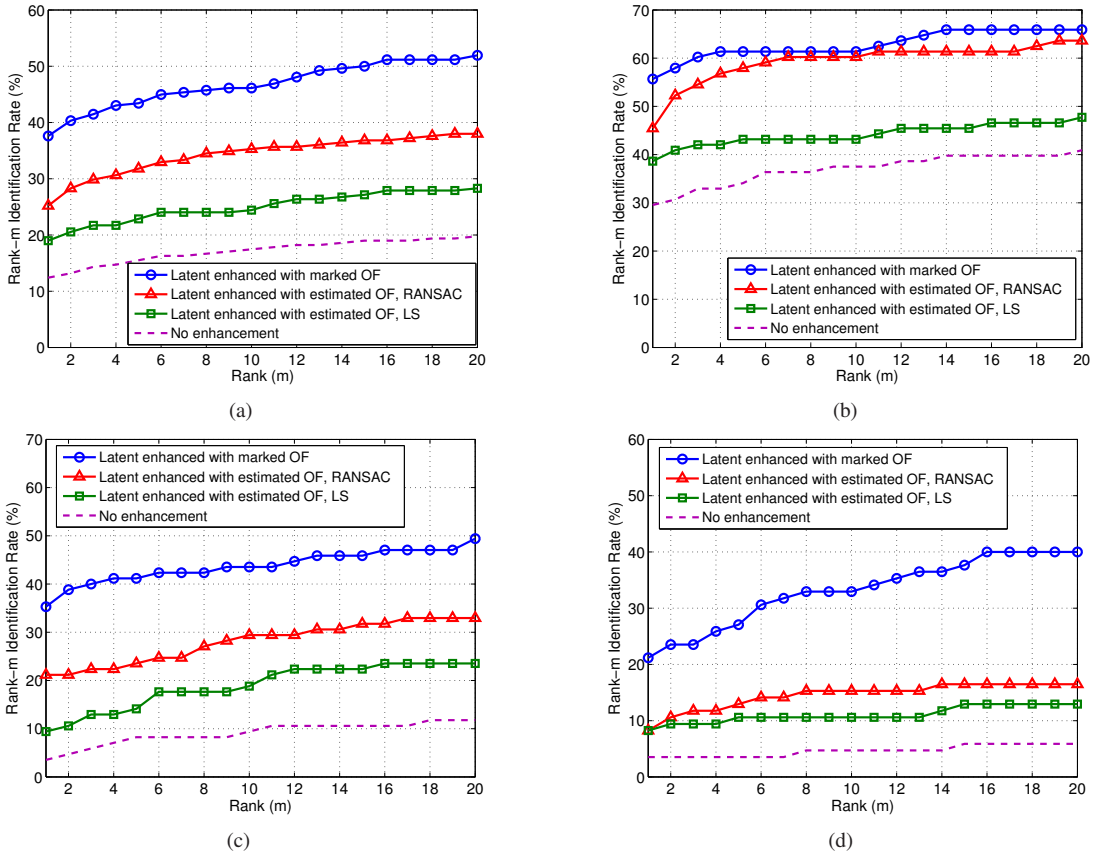

Figure 10. CMC curves. (a) All latents, (b) good quality latents, (c) bad quality latents, and (d) ugly quality latents.

the proposed algorithm achieved performance close to the upper bound (manually marked orientation field; see Fig. 10b). For bad and ugly quality latents, while the proposed algorithm performs much better compared to least-squares estimation method or no enhancement case (see Figs. 10c and d), there is a significant gap in performance between the proposed algorithm and the upper bound. This shows that the automatic orientation field estimation in very poor quality latents is still challenging.

Fig. 11 shows four successful examples where the proposed enhancement algorithm improved the match score with the mated rolled fingerprint. In these four cases, the mated rolled print can be retrieved at a high rank from the large database of 27,258 images. Fig. 12 shows a failure case where the failure in orientation field estimation leads to a lower genuine match score after enhancement.

4. Conclusions and Future Work

Latent fingerprints found at crime scenes provide crucial evidence to law enforcement agencies. The latents are typically searched against a large fingerprint database which is the collection of rolled/plain fingerprints of previously apprehended criminals. Due to the poor quality of the latents, latent examiners perform manual feature markup and visual verification between the latent and the candidate fingerprints from the database. A "Lights-Out" mode for latent identification is desired to reduce the burden on latent examiners and to introduce a level of consistency in fingerprint matching, particularly in searching ever growing fingerprint database.

We proposed a latent fingerprint enhancement algorithm which only requires minimal markup (ROI and singular points) to improve the automatic matching accuracy. The orientation field of the latents is estimated by R-RANSAC which is effectively used to find a correct orientation field model in the presence of noise and distortion. The estimated orientation field is used to enhance ridge structures by Gabor filtering. The proposed algorithm significantly improved the matching performance of a commercial matcher when the enhanced latents are fed into the matcher.

We propose to extend our work as follows:

- Improve the performance of the orientation field estimation algorithm for bad and ugly quality latents in NIST SD27.
- Reduce the human markup even further; ideally, the input of the algorithm should only be the latent image.

- Assess the quality of the latents automatically. The reliability of the features extracted from the latents can be adjusted according to the quality to automatically determine the degree of human intervention for feature markup and improve the overall matching accuracy.

Acknowledgements

This research was supported by grants from the NSF Center for Identification Technology Research (CITeR) and the FBI's Biometric Center of Excellence. This research was also partially supported by WCU (World Class University) program funded by the Ministry of Education, Science and Technology through the National Research Foundation of Korea (R31-10008).

References

[1] Evaluation of latent fingerprint technologies 2007. `http://fingerprint.nist.gov/latent/elft07/`.

[2] A. M. Bazen and S. H. Gerez. Systematic methods for the computation of the directional fields and singular points of fingerprints. *IEEE Trans. Pattern Analysis and Machine Intelligence*, 24(7):905–919, 2002.

[3] E. Blotta and E. Moler. Fingerprint image enhancement by differential hysteresis processing. *Forensic Science International*, 141(2):109–113, 2004.

[4] S. Chikkerur, A. N. Cartwright, and V. Govindaraju. Fingerprint enhancement using STFT analysis. *Pattern Recognition*, 40(1):198–211.

[5] M. A. Fischler and R. C. Bolles. Random sample consensus: A paradigm for model fitting with applications to image analysis and automated cartography. *Communications of the ACM*, 24(6):381–396, 1981.

[6] L. Hong, Y. Wan, and A. K. Jain. Fingerprint image enhancement: Algorithm and performance evaluation. *IEEE Trans. Pattern Analysis and Machine Intelligence*, 20(8):777–789, 1998.

[7] M. Indovina, R. A. Hicklin, and G. I. Kiebuzinski. Evaluation of latent fingerprint technologies: Extended feature sets [evaluation #1]. NISTIR 7775, March 2011.

[8] J. Matas and O. Chum. Randomized RANSAC with $t_{d,d}$ test. *Image and Vision Computing*, 22(10):837–842, 2004.

[9] B. G. Sherlock and D. M. Monro. A model for interpreting fingerprint topology. *Pattern Recognition*, 26(7):1047–1055, 1993.

[10] C. Wilson. Fingerprint vendor technology evaluation 2003: Summary of results and analysis report. NISTIR 7123, June 2004.

[11] S. Yoon, J. Feng, and A. K. Jain. On latent fingerprint enhancement. In *Proceedings of SPIE, Biometric Technology for Human Identification VII*, volume 7667, pages 766707_01–766707_10, 2010.

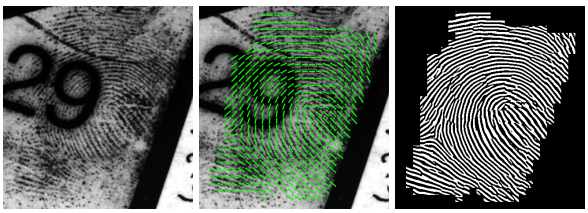

(a) Good quality latent (G019): {4,5277}→{54,1}

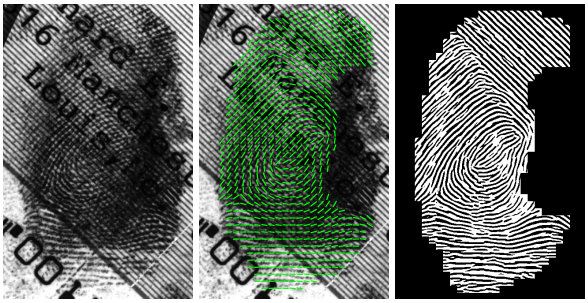

(b) Good quality latent (G027): {1,4714}→{22,1}

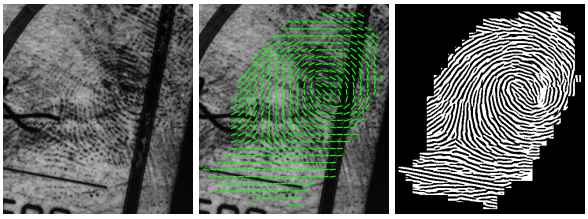

(c) Bad quality latent (B142): {3,1253}→{34,1}

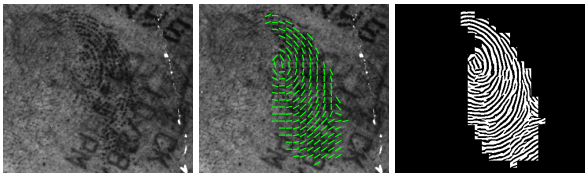

(d) Ugly quality latent (U282): {0,27258}→{24,1}

Figure 11. Successful examples where the proposed algorithm improves the matching performance. Left: latent, Center: estimated orientation field, and Right: binarized enhanced image. Match score of the latent with the mated rolled print and its retrieval rank from a database of 27,258 rolled prints are shown as: {score, rank} before enhancement → {score, rank} after enhancement.

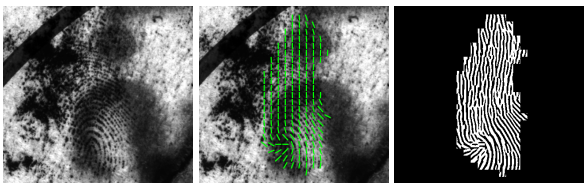

Figure 12. Failure case (G029). Due to the failure in orientation field estimation, the match score drops from 23 (before enhancement) to 3 (after enhancement), and the retrieval rank for the true mate is increased from 12 to 15801.